Optics Letters

Dispersion engineering and thermo-optic tuning in mid-infrared photonic crystal slow light waveguides on silicon-on-insulator

YIMING MA,[1,2,3] BOWEI DONG,[1,3] BO LI,[1,3] KAH-WEE ANG,[1] AND CHENGKUO LEE[1,2,3,*]

[1]Department of Electrical and Computer Engineering, National University of Singapore, Singapore 117576, Singapore
[2]NUS Suzhou Research Institute (NUSRI), Suzhou Industrial Park, Suzhou 215123, China
[3]Center for Intelligent Sensors and MEMS, National University of Singapore, Singapore 117608, Singapore
*Corresponding author: elelc@nus.edu.sg

Received 19 September 2018; accepted 4 October 2018; posted 9 October 2018 (Doc. ID 346261); published 5 November 2018

In this Letter, the design, fabrication, and characterization of slow light devices using photonic crystal waveguides (PhCWs) in the mid-infrared wavelength range of 3.9–3.98 µm are demonstrated. The PhCWs are built on the silicon-on-insulator platform without undercut to leverage its well-developed fabrication process and strong mechanical robustness. Lattice shifting and thermo-optic tuning methods are utilized to manipulate the slow light region for potential spectroscopy sensing applications. Up to 20 nm wavelength shift of the slow light band edge is demonstrated. Normalized delay-bandwidth products of 0.084–0.112 are obtained as a result of dispersion engineering. From the thermo-optic characterization results, the slow light enhancement effect of thermo-optic tuning efficiency is verified by the proportional relationship between the phase shift and the group index. This work serves as a proof of concept that the slow light effect can strengthen light–matter interaction and thereby improve device performance in sensing and nonlinearity applications.

https://doi.org/10.1364/OL.43.005504

Mid-infrared (MIR) silicon photonics (SiP) has been attracting more and more attention due to its potential for chemical and biological sensing applications. The MIR wavelength range extensively overlaps with the functional group regions as well as fingerprint regions of various organic and inorganic compounds, promoting label-free and surface-functionalization-free selective sensing based on absorption spectroscopy [1,2]. In addition, in the MIR range, the two- and three-photon absorption in silicon becomes negligible, permitting higher-power density transmission than at the telecom wavelengths, which benefits nonlinearity phenomenon generation [3]. Various SiP material platforms, including silicon-on-insulator (SOI) [4], silicon-on-sapphire [5], silicon-on-nitride [6], silicon-on-calcium-fluoride [7], as well as silicon-on-lithium-niobate [8], have been demonstrated in MIR with low loss and favorable performance. Among these material platforms, SOI is undoubtedly the most popular one owing to its fabrication maturity and stability. Although the absorption loss caused by silicon dioxide (SiO_2) cladding starts to increase from 3.6 µm onward [9], recent research has confirmed that SOI remains a promising candidate up to 3.8 µm due to the high optical mode confinement enabled by the high refractive index contrast between Si and SiO_2 [10,11]. Moreover, we have demonstrated a SOI channel waveguide in our previous work with propagation loss as low as 2 dB/cm in the wavelength range of 3.68–3.88 µm [12].

Slow light with remarkably low group velocity offers the possibility for spatial compression of optical energy, which reduces device footprint and enhances light–matter interaction [13]. Therefore, slow light is regarded as one of the most promising techniques for improving device performance in sensing and nonlinearity applications [14–17]. Photonic crystal waveguide (PhCW), as one of the most popular slow light structures, has been demonstrated on SOI in the wavelength region between 2.9 and 3.9 µm [18]. In this work, silicon dioxide (SiO_2) below the PhC slab was removed to suppress the absorption loss. However, the fabrication yield of such a suspended membrane structure is low, and the weak mechanical robustness hinders its use for sensing applications. More importantly, the slow light performance of this device is limited because of the lack of dispersion engineering, the purpose of which is to achieve nearly constant group index over a wide bandwidth. In addition to dispersion engineering by tailoring the PhCW geometry, thermo-optic tuning is another feasible approach to manipulate the slow light properties thanks to the inherent high thermo-optic coefficient of Si. From another perspective, the thermo-optic tuning efficiency is also enhanced by the slow light effect through the improvement of light–matter interaction. Although such an enhancement effect has been reported in near-infrared PhCWs integrated with microheaters [19–21], the relationship between the phase shift induced by thermo-optic tuning and the group index has not been thoroughly studied with the support of experimental results.

In this Letter, we experimentally demonstrate for the first time, to the best of our knowledge, PhCW with dispersion-engineered slow light effect in the MIR wavelength range of 3.9–3.98 μm on a SOI platform without undercut. This wavelength range extensively overlaps with a characteristic absorption peak of nitrous oxide (N_2O), a gas that has significant uses in medicine, engineering, and so forth [22]. Lattice shifting and thermo-optic tuning methods are employed to manipulate the slow light region to match it with different positions on the characteristic absorption peak, providing high potential in absorption spectroscopy applications. From the thermo-optic tuning results, a proportional relationship between the phase shift and the group index is verified, which agrees well with the theoretical prediction and serves as a proof of concept that the slow light effect can strengthen light–matter interaction, forecasting the improvement of performance in sensing and nonlinearity applications using our MIR PhCW slow light devices.

Figure 1(a) illustrates the schematic drawing of the SOI MIR slow light device. The PhCW is embedded into one arm of a Mach–Zehnder interferometer (MZI). We name this arm the signal arm (SA) and the other the reference arm (RA). The light from a tunable MIR laser (Daylight MidCat, 3.64–4.12 μm) is coupled into the Si waveguide through a linearly tapered butt coupler at the edge of the chip. The coupled light is maintained in single mode profile and equally divided into RA and SA through a Y-junction, then recombined by another Y-junction and coupled to another fiber through the output butt coupler. Optical lithography is utilized to fabricate the devices, and the process is clearly stated in our previous work [23]. The fabrication starts from a 220 nm SOI wafer. To support MIR propagation mode, a 180 nm thick Si layer is epitaxially deposited. The optical loss due to the interface between the single crystal Si and epitaxy Si is negligible in the 3.4–4.2 μm range based on our testing results shown in [12]. After the etching of the Si device layer, 3 μm thick SiO_2 is deposited, followed by chemical mechanical polishing to obtain a planarized 2 μm thick upper cladding layer, which is sufficient to optically isolate the air cladding or metallic heater above. Figure 1(b) shows the scanning electron microscope (SEM) image of the fabricated PhCW. The middle row of holes in the light propagation direction is removed. The dispersion-engineered lattice constant and hole diameter are chosen to be 1.183 μm and 800 nm based on simulation, respectively. The overall length of the PhCW is 61 μm. The inset in Fig. 1(b) shows the profile of transverse-electrical-like (TE-like) y-even gap-guided mode propagating in the PhCW, which is simulated through the plane wave expansion method using MIT photonic bands (MPBs). Most of the mode energy is well confined in the line-defect of the PhCW.

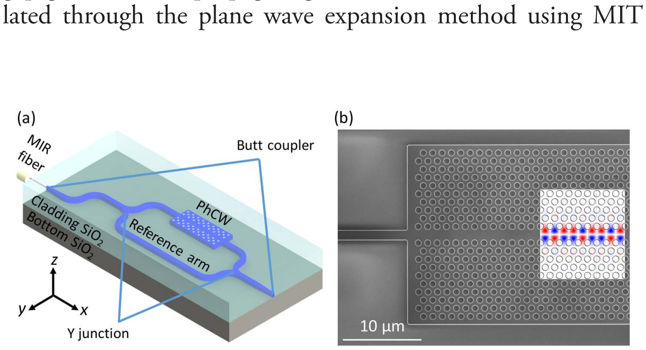

Fig. 1. (a) Schematic illustration of SOI MIR slow light MZI with PhCW embedded into one arm of it. (b) SEM image of fabricated PhCW without lattice shift. The inset shows the propagation mode profile.

The testing setup and procedure also can be found in our previous work [23]. The two arms of the MZI have the same physical length but different group indices. The constructive interference fringes appear more densely as the group index difference between the RA and SA increases, which results in a decreasing free spectral range (FSR) in the MZI transmission spectrum. Figures 2(a), 2(b), and 2(c) illustrate the measurement and simulation results of three MZIs integrated with PhCW, in which the first row of holes is shifted along the light propagation direction by 0, 50, and 100 nm, respectively. Compared with changing hole size, the lattice shifting method possesses better fabrication robustness, and thus is chosen for further dispersion engineering. The FSR changes are clearly observed in the measurement and match well with the three-dimensional (3D) finite difference time domain (FDTD) simulation results using Lumerical FDTD Solutions. Beyond the band edge wavelength, the simulation results show constant transmission values, which means the PhCW fully blocks all the incoming light and the MZI behaves like a pure strip waveguide. In the measurement results, resonance fringes with nearly constant FSR appear beyond the band edge and in the fast light region (on the left of the gray dashed line), which is caused by the Fabry–Perot resonance between the two coupling facets. The band edge blueshifts 8 nm in the case of a 100 nm lattice shift, compared with its wavelength when there is no lattice shift. The group index can be extracted from the MZI transmission spectrum using the following equation [19]:

$$n_g(\lambda) = n_g^{\mathrm{ref}}(\lambda) + \frac{\lambda_{\max}\lambda_{\min}}{2L|\lambda_{\max} - \lambda_{\min}|}, \quad (1)$$

where $\lambda_{\max}$ and $\lambda_{\min}$ are the wavelengths of two adjacent constructive and deconstructive interference fringes, respectively. L is the length of the PhCW. n_g^{ref} is the group index of the reference strip waveguide. The calculated group indices of

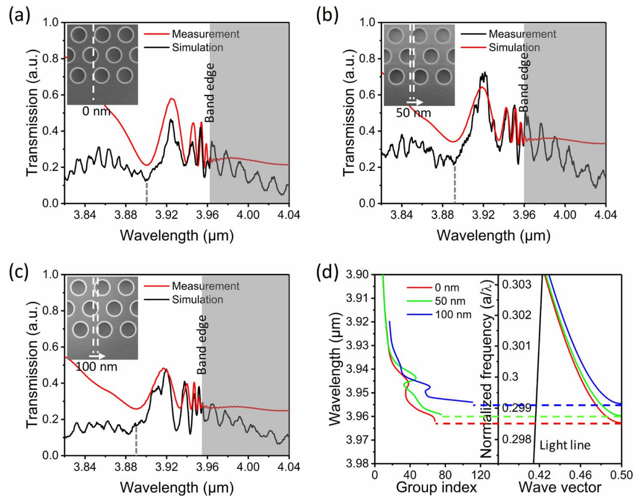

Fig. 2. (a)–(c) Measured and simulated transmission spectra of MZIs integrated with PhCW (a) without lattice shift, (b) with 50 nm lattice shift, and (c) with 100 nm lattice shift. The insets show the SEM images of the corresponding PhCWs. (d) Group index curves of the three lattice shift designs together with the simulated dispersion curves. The dotted lines indicate their agreement on the band edge positions.

the PhCW are connected using smooth curves and plotted in Fig. 2(d). The group index increases dramatically with the wavelength approaching the band edge. The maximum measurable group index is limited by the resolution of our laser source (~200 pm). The group index increases with rising lattice shift. The simulated dispersion curve of the propagating mode is also depicted in Fig. 2(d). The normalized frequency in the y-axis is calculated with the lattice constant of 1.183 μm and matched with the wavelength axis in the left. The slope of the dispersion curve represents the group velocity. The band curve becomes flatter, representing slow (or stopped) light near (or at) the band edge. The dashed lines show that the measured group index curves of the three lattice shift designs of PhCW all agree well with the simulated dispersion curves in terms of the band edge positions.

To realize thermo-optic tuning of our PhCW slow light device, a microheater made of titanium nitride (TiN) is deployed above the Si PhC slab, as illustrated in Fig. 3(a). Figure 3(b) shows the microscopic image of the fabricated microheater. The microheater is designed to be S-shaped across the entire Si PhC slab to ensure good uniformity of the heat dispensation. The resistance of the microheater is measured to be 7 kΩ, and the current supplied to the microheater ranges from 0to 3 mA. As shown in Figs. 3(c) and 3(d), the temperature distributions simulated by the finite element method using COMSOL Multiphysics have good uniformity over the entire PhC slab and along the line-defect of the PhCW. While the lattice shifting method is deployed to blueshift the band edge, on the contrary, heating up the PhCW will increase the refractive index (RI) of Si and redshift the slow light region. Leveraging these two methods together, we can achieve large spectrum range tuning of our devices and hence ensure the RI change and characteristic absorption to happen in the maximum efficiency range. Figure 4(a) shows the transmission spectra of the MZI under different values of applied current, where the PhCW embedded into it is without lattice shift. The phase shifts of the constructive and deconstructive interference fringes in

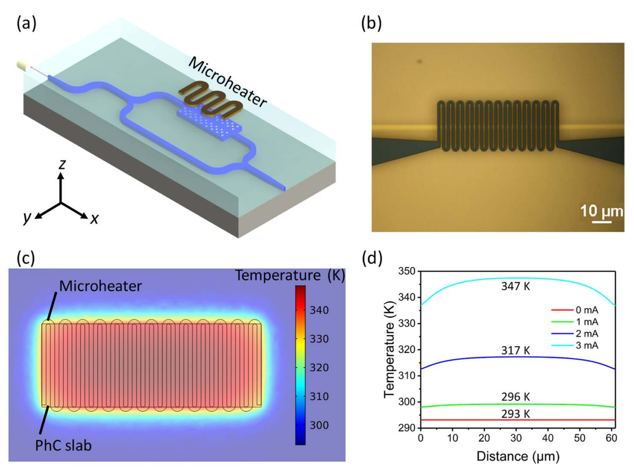

Fig. 3. (a) Schematic illustration of SOI MIR slow light MZI integrated with microheater. (b) Microscopic image of fabricated PhCW with microheater above. (c) Simulated temperature distribution over the PhC slab under 3 mA applied current. (d) Simulated temperature distribution along the line-defect of PhCW under different magnitude of applied currents.

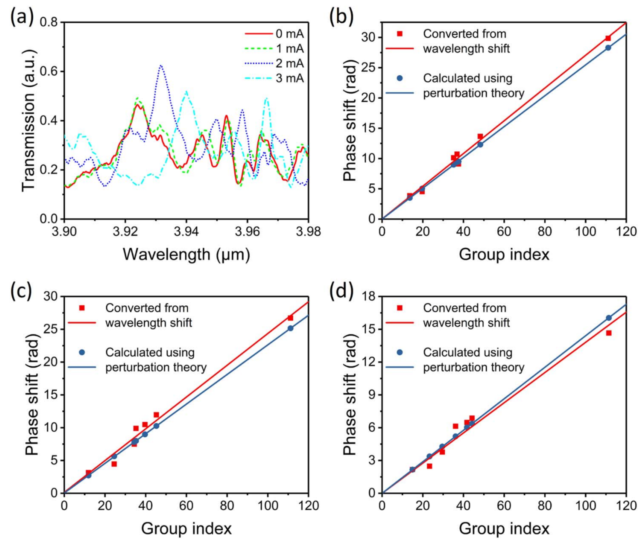

Fig. 4. (a) MZI transmission spectra under different values of applied current. (b)–(d) Plots of phase shifts at the interference fringes converted from wavelength shift and calculated using perturbation theory as a function of group index, when the applied current changes (b) from 0 to 3 mA, (c) from 1 to 3 mA, and (d) from 2 to 3 mA.

the spectra can be converted from their wavelength shifts. At constructive interference fringes we have

$$\frac{2\pi}{\lambda}(n_\lambda - n_\lambda^{\mathrm{ref}})L = 2k\pi, \tag{2}$$

where λ is the wavelength of the constructive interference fringe before heating, k is a positive integer, and n_λ and n_λ^{ref} are the effective RIs of the PhCW and the reference strip waveguide at the wavelength of λ, respectively. When the phase shift $\Delta\varphi$ is induced to the SA of the MZI, we can achieve that

$$\frac{2\pi}{\lambda+\Delta\lambda}(n_{\lambda+\Delta\lambda} - n_{\lambda+\Delta\lambda}^{\mathrm{ref}})L + \Delta\varphi = 2k\pi, \tag{3}$$

where $\Delta\lambda$ is the wavelength shift, and $n_{\lambda+\Delta\lambda}$ and $n_{\lambda+\Delta\lambda}^{\mathrm{ref}}$ are the effective refractive indices of the PhCW and the reference strip waveguide at the wavelength of $\lambda+\Delta\lambda$, respectively. Combining Eqs. (2) and (3) we have

$$\Delta\varphi = 2\pi L\left(\frac{n_\lambda - n_\lambda^{\mathrm{ref}}}{\lambda} - \frac{n_{\lambda+\Delta\lambda} - n_{\lambda+\Delta\lambda}^{\mathrm{ref}}}{\lambda+\Delta\lambda}\right). \tag{4}$$

We denote $f(\lambda) = (n - n^{\mathrm{ref}})/\lambda$. Then according to the definition of group index ($n_g = n - \lambda dn/d\lambda$), we have its first order derivative to be $f'(\lambda) = (-n_g + n_g^{\mathrm{ref}})/\lambda^2$. Thus Eq. (4) can be approximated as

$$\Delta\varphi = 2\pi L * f'(\lambda) * (-\Delta\lambda) = 2\pi L * \frac{n_g - n_g^{\mathrm{ref}}}{\lambda^2} * \Delta\lambda. \tag{5}$$

For deconstructive interference fringes, the only difference is the $2k\pi$ in Eqs. (2) and (3) replaced by $2(k+1)\pi$. Therefore, a relationship equation between the phase shift and the wavelength shift the same as Eq. (5) can be derived. Using Eq. (5), the phase shifts of every interference fringe can be extracted from the MZI transmission spectra. According to perturbation theory, the phase shift induced in a PhCW is also given by [24]

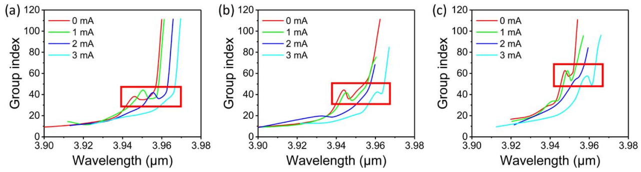

Fig. 5. Group index curves of PhCWs (a) without lattice shift, (b) with 50 nm lattice shift, and (c) with 100 nm lattice shift, under different magnitude of applied currents.

$$\Delta\varphi = 2\pi L * \frac{\Delta n \sigma n_g}{n\lambda}, \tag{6}$$

where σ is the fraction of the optical mode energy confined in Si, n is the RI of Si, and Δn is the Si RI change caused by heating. σ is calculated from the mode profile simulated using MPB at the wavelength of each fringe. n and as a result Δn are obtained from the surface fitting of the recommended values on the RI of Si in [25] corresponding to the simulated temperature values indicated in Fig. 3(d). The phase shift at every interference fringe is separately calculated using Eqs. (5) and (6) and plotted as a function of the group index in the same diagram. Figures 4(b), 4(c), and 4(d) show the aggregated plots in the case of the applied current changed from 0 to 3 mA, from 1 to 3 mA, and from 2 to 3 mA, respectively. It is seen that no matter how much the applied current changes, the phase shift converted from wavelength shift agrees well with that calculated using perturbation theory at every interference fringe, which follows a proportional relationship with the group index over the relatively short wavelength range of the slow light region. It is evident that the thermo-optic tuning efficiency is enhanced by the slow light effect.

Figure 5 illustrates the group index curves of the three lattice shift designs of PhCW calculated using Eq. (1) under local heating by the microheater with different magnitudes of applied currents. The dispersion compensated (DC) regions are marked by red boxes. The slightly oscillating group index in the DC region indicates relatively low group velocity dispersion, which suppresses signal distortion. Also because of the nearly constant group index, such a region redshifts while its slow light properties basically remain unchanged. The bandwidth and the average group index are defined consistently with our previous work [23]. The 0, 50, and 100 nm lattice shift designs are observed with average group index of around 40, 45, and 60 and bandwidth of about 11, 10, and 6 nm, respectively. Corresponding normalized delay–bandwidth products (NDBPs) are calculated to be 0.084–0.112, which significantly exceed that of the reported MIR PhCW without dispersion engineering [18].

In conclusion, we experimentally demonstrated dispersion-engineered PhCW slow light devices in the MIR wavelength range of 3.9–3.98 μm on the most mature and robust SOI platform without undercut. Lattice shifting, as well as thermo-optic tuning methods, were deployed to manipulate the slow light band edge. A 20 nm tuning range consisting of 8 nm blueshift with 100 nm lattice shift and 12 nm redshift with 3 mA applied current was demonstrated. NDBPs of 0.084–0.112 were achieved, which significantly surpass that of the reported MIR PhCW without dispersion engineering. Moreover, the proportional relationship between the phase shift and the group index was verified through the analysis of the thermo-optically tuned MZI transmission spectra. This work is evidence showing that the slow light effect enhances light–matter interaction, which can be exploited for improving device performance in sensing and nonlinearity applications.

Funding. National Research Foundation Singapore (NRF) (NRF-CRP15-2015-02); NRF-ISF Joint Research Grant (NRF-ISF) (NRF2015-NRF-ISF001-2620); National Natural Science Foundation of China (NSFC) (61474078).

Acknowledgment. Mr. Yiming Ma appreciates financial support from the NUS-NUSRI Research Scholarship.

REFERENCES

1. T. Hu, B. Dong, X. Luo, T.-Y. Liow, J. Song, C. Lee, and G.-Q. Lo, Photon. Res. **5**, 417 (2017).
2. P. T. Lin, S. W. Kwok, H. G. Lin, V. Singh, L. C. Kimerling, G. M. Whitesides, and A. Agarwal, Nano Lett. **14**, 231 (2014).
3. B. Jalali, Nat. Photonics **4**, 506 (2010).
4. M. Nedeljkovic, A. V. Velasco, A. Z. Khokhar, A. Delage, P. Cheben, and G. Z. Mashanovich, IEEE Photon. Technol. Lett. **28**, 528 (2016).
5. T. Baehr-Jones, A. Spott, R. Ilic, A. Spott, B. Penkov, W. Asher, and M. Hochberg, Opt. Express **18**, 12127 (2010).
6. S. Khan, J. Chiles, J. Ma, and S. Fathpour, Appl. Phys. Lett. **102**, 121104 (2013).
7. Y. Chen, H. Lin, J. Hu, and M. Li, ACS Nano **8**, 6955 (2014).
8. J. Chiles and S. Fathpour, Optica **1**, 350 (2014).
9. R. Soref, Nat. Photonics **4**, 495 (2010).
10. M. M. Milošević, M. Nedeljkovic, T. M. Ben Masaud, E. Jaberansary, H. M. H. Chong, and M. M. Milo, Appl. Phys. Lett. **101**, 121105 (2012).
11. M. Nedeljkovic, A. Z. Khokhar, Y. Hu, X. Chen, J. S. Penades, S. Stankovic, H. M. H. Chong, D. J. Thomson, F. Y. Gardes, G. T. Reed, and G. Z. Mashanovich, Opt. Mater. Express **3**, 1205 (2013).
12. B. Dong, X. Guo, C. P. Ho, B. Li, H. Wang, C. Lee, X. Luo, and G. Q. Lo, IEEE Photon. J. **9**, 4501410 (2017).
13. T. Baba, Nat. Photonics **2**, 465 (2008).
14. W.-C. Lai, S. Chakravarty, Y. Zou, and R. T. Chen, Opt. Lett. **38**, 3799 (2013).
15. K. Qin, S. Hu, S. T. Retterer, I. I. Kravchenko, and S. M. Weiss, Opt. Lett. **41**, 753 (2016).
16. A. Brimont, D. J. Thomson, P. Sanchis, J. Herrera, F. Y. Gardes, J. M. Fedeli, G. T. Reed, and J. Martí, Opt. Express **19**, 20876 (2011).
17. B. Corcoran, C. Monat, C. Grillet, D. J. Moss, B. J. Eggleton, T. P. White, L. O'Faolain, and T. F. Krauss, Nat. Photonics **3**, 206 (2009).
18. C. Reimer, M. Nedeljkovic, D. J. M. Stothard, M. O. S. E. C. Reardon, L. O'Faolain, M. Dunn, G. Z. Mashanovich, and T. F. Krauss, Opt. Express **20**, 29361 (2012).
19. Y. A. Vlasov, M. O'Boyle, H. F. Hamann, and S. J. McNab, Nature **438**, 65 (2005).
20. N. Ishikura, R. Hosoi, R. Hayakawa, T. Tamanuki, and M. Shinkawa, Appl. Phys. Lett. **100**, 221110 (2012).
21. S. Yan, X. Zhu, L. H. Frandsen, S. Xiao, N. A. Mortensen, J. Dong, and Y. Ding, Nat. Commun. **8**, 14411 (2017).
22. S. E. Stein, in *NIST Chemistry WebBook, NIST Standard Reference Database Number 69* (National Institute of Standards and Technology, 2018).
23. Y. Ma, B. Dong, B. Li, J. Wei, Y. Chang, C. P. Ho, and C. Lee, IEEE J. Sel. Top. Quantum Electron. **24**, 6101608 (2018).
24. M. Soljačić and J. D. Joannopoulos, Nat. Mater. **3**, 211 (2004).
25. H. H. Li, J. Phys. Chem. Ref. Data **9**, 561 (1980).